Parkinsonian tremor identification with multiple local field potential feature classification

Eduard Bakstein[a*], Jonathan Burgess[b], Kevin Warwick[b], Virginie Ruiz[b], Tipu Aziz[c, d], John Stein[d]

[a] *Department of Cybernetics, Czech Technical University, Prague, Czech Republic*

[b] *Department of Systems engineering, University of Reading, UK*

[c] *The Functional Neurosurgery Group, Department of Surgery, John Radcliffe Hospital, Oxford, UK*

[d] *University Laboratory of Physiology, University of Oxford, UK*

[*] *Corresponding author: Eduard Bakstein, eduard.bakstein@fel.cvut.cz, Dept. of Cybernetics, FEL CVUT, Karlovo nam. 13, 12135, Czech Republic*

Number of text Pages:31

Number of Figures:3

Number of Tables:3

Abstract

This paper explores the development of multi-feature classification techniques used to identify tremor-related characteristics in the Parkinsonian patient. Local field potentials were recorded from the subthalamic nucleus and the globus pallidus internus of eight Parkinsonian patients through the implanted electrodes of a Deep brain stimulation (DBS) device prior to device internalization.

A range of signal processing techniques were evaluated with respect to their tremor detection capability and used as inputs in a multi-feature neural network classifier to identify the activity of Parkinsonian tremor. The results of this study show that a trained multi-feature neural network is able, under certain conditions, to achieve excellent detection accuracy on patients unseen during training. Overall the tremor detection accuracy was mixed, although an accuracy of over 86% was achieved in four out of the eight patients.

Keywords

Parkinson's disease

Local field potentials

Deep brain stimulation

Multiple features

Feature extraction

Neural networks

Highlights

- Design of a pattern detection system for Parkinson's disease tremor.
- Detection uses processing of LFP signals from the stimulation electrodes.
- The system was based on Neural Network using multiple feature types.
- Satisfactory results were obtained for a subgroup of tested patients

Abbreviations

DBS – Deep brain stimulation

LFP – Local Field potentials

NN – Neural Networks

PD – Parkinson's disease

STN – Subthalamic nucleus

GPi - Globus pallidus internus

EMG – Electromyography

PDF – Probability Density Function

FFT – Fast Fourier Transform

PSD – Power Spectrum Density

1 Introduction

Parkinson's Disease (PD) is a chronic progressive neurodegenerative movement disorder, which is estimated to affect 6.3 million people worldwide (Baker and Graham, 2004) and for which there is no recognised cure. The pathophysiology of PD is idiosyncratic in nature resulting in a variety of symptoms displayed by patients, the cardinal clinical symptoms of which are bradykinesia, postural instability, and most notably, rest tremor (Rajput and Birdi, 1997). The frequency of a Parkinsonian tremor does not refer to the firing rate of muscle fibres but the movement of the limb as a whole. This individual frequency is predominantly exhibited from 4 to 9 Hz and in the context of muscular movement it is referred to as the tremor frequency (Carr, 2002; Deuschl et al., 1998).

Parkinsonian tremor has been reported to be driven by the abnormal activity of neural signals propagated throughout the sensorimotor system (Hammond et al., 2007; Morrison et al., 2008), which we aimed to identify in this study. The recorded LFP signal represents low frequency components originating from axons, somata and dendrites around the electrode, and thus mainly reflects the input to the local brain region. The exact frequency range of the LFP is, in general, below 100 Hz (Brown, 2003). However, the majority of neurophysiological studies on Parkinsonian patients have focussed on LFP oscillations in the range of 5 to 35 Hz (Steigerwald et al., 2008; Trottenberg et al., 2007). Current biomarkers for Parkinsonian tremor analyse the oscillations of the LFP signal. The most commonly studied neural activity in the LFP is that of the tremor and beta frequency bands.

It has been found that some groups of STN and GPi neurons display tremor-related bursts with a high coherence to the frequency of spontaneous muscular tremor(Amtage et al., 2008). Such neuron pairs are commonly termed 'tremor cells'. Synchronized tremor activity is not clearly understood and it is presently unknown as to whether the activity of tremor cells contributes to the development of tremor or is simply an artefact driven by the physical tremor. The presence of tremor cells and the activity of the beta band are however known to be bound to Parkinsonian tremor (Amtage et al., 2008; Zaidel et al., 2010). The results dispel the belief that tremor cells are a manifestation of purely the lack of dopamine, yet still the threat of a physical artefact cannot be ignored. Overall, these investigations

suggest the pathophysiology of PD is in close relation to the changes apparent in STN activity.

Apart from tremor-related activity in the STN and GPi nuclei, thalamus and cortex are often related to the mechanism of tremor. Previous studies have shown, that LFP recordings from these sites show correlation with muscular (EMG) activity (Marsden et al., 2000). However, as the majority of DBS implants are nowadays placed either in the STN or GPi nuclei, the focus of this study is aimed at LFP signals from these regions.

A number of studies have shown significant coherence between tremor cells and EMG activity in the STN at the tremor frequency (Rodriguez et al., 1998). The tremor frequency and beta frequency have been of great interest in previous studies (Lemstra et al., 1999; Marceglia et al., 2009), and are reported to be akinetic, i.e. inversely related to motor activity. Some studies discuss the coherence between beta activity and common symptoms of Parkinson's disease, such as akinesia or rigidity. Also, they have been reported to be strongly modulated by voluntary movement activity and medication. The range of the tremor frequency varies between studies. In the context of muscular activity a range of 4 - 9 Hz is common, however neurophysiological studies analysing LFP signals tend towards lower frequencies (3.0 - 4.5 Hz (Wang et al., 2007) and 3.0 - 6.0 Hz (Lemstra et al., 1999)).

The beta-band is a range of frequencies between 12 and 30 Hz and is used in neuroscience to describe the oscillatory range of brain activity. Beta-band synchronisation between neuron pairs in the thalamus has been reported in the majority of investigations into Parkinsonian tremor (Amtage et al., 2008; Levy et al., 2002). It has already been demonstrated that beta activity has a direct impact on post-surgical prognosis, i.e. electrophysiological factors bearing direct relevance to surgical outcome (Marsden et al., 2001; Ray et al., 2009a; Zaidel et al., 2010). This may in the future be detected pre-operatively through non-invasive imaging techniques, e.g. (Ray et al., 2009b). Further, high-frequency stimulation has been shown to suppress subcortical beta activity (Kuhn et al., 2008). Activity in the beta range of the STN has also been found to be a strong marker for the sensory-motor region of the STN and was successfully used to identify this area in Microelectrode recordings (Zaidel et al., 2009).

Wang et al. reported on a coherent relationship between the onset of PD tremor and LFP oscillation activity, in both tremor (3.0-4.5 Hz) and beta-band (10-30 Hz) frequencies (Wang et al., 2005). Coherence was evident between LFP and EMG signals at the tremor frequency, whereas the power exhibited at the beta-band frequencies decreased prior to and throughout tremor activity.

Given the idiosyncratic nature of the disease we propose here that to achieve a high rate of tremor classification over a broad range of patients, a concise biomarker will benefit from exploring more than just the frequency feature of the LFP. To improve upon current biomarkers, we therefore explore here a multi-feature classification approach to identify Parkinsonian tremor within an LFP signal.

Selective properties of individual features from the temporal and spectral domain were tested in the study with optimal properties being used for the classification of tremor. Moreover, the suitability and relevance of the different approaches was compared. The classification results were then used to assess the actual applicability of the proposed method. As a result of this, features suitable for tremor detection can be differentiated from features with little or no significance to the problem. The results obtained in this study further our understanding of Parkinsonian tremor and ultimately will enhance the maintenance of personal health.

2 Materials and Methods

In this section we have summarized the range of experimental design procedures carried out in terms of recording signals, conditioning signals and evaluating the classification of system performance.

The overall task requirements were as follows: Firstly simultaneous LFP and EMG recordings were made using volunteer patients with implanted deep brain electrodes. Secondly the data obtained – particularly deep brain LFPs – were divided into smaller chunks (windows) and different features were measured, these included temporal features, spectral features and features founded on information theory. Thirdly feedforward Neural Networks were trained using only a subset of data based on the leave one out philosophy, the one left out being the patient whose data would be subsequently analysed. This made it

as difficult as possible for the overall analysis to investigate each patient as it had to do so without seeing any data from that particular patient apriori. Apriori viewing, and even training on a particular patient's data would have made the subsequent results appear to be far better than those actually obtained – in this case the subsequent results should be seen as ' worst case' outputs.

As each of the features are introduced, reasons are given, based both on previous research and subsequent analysis as to why each feature was considered. In any case, in the results section it will be seen that any of the features which didn't actually turn out to be particularly useful were effectively dropped. The list here should therefore seen to be one which includes all reasonable possibilities. For the neural networks and signal transformations, concepts of their employment are described.

2.1 Subjects and data acquisition

Eight volunteering patients, who had been diagnosed with tremor-dominant idiopathic PD, participated in this study as they were undergoing surgical DBS treatment at the John Radcliffe Hospital (JRH), Oxford, UK at the time. Postoperative magnetic resonance imaging confirmed the successful implantation of the DBS electrode lead(s) (Medtronics© 3387) within the target region.

We exploited the external bi-directional connection to the electrodes, which was available during the intra-operative period of stereotactic surgery, to record neural and coherent muscular signals from all of the volunteering patients. Approval for the recording sessions was granted by the local research ethics committee of the Oxfordshire Health Authority, UK, and informed consent was obtained from each volunteer.

The DBS electrode lead employed was Medtronic 3387, with four electrodes spaced 1.5 mm apart which permits three different contact pair configurations (0+1, 1+2, and 2+3) to be simultaneously recorded in a bipolar fashion with one contact used as reference. Muscular (EMG) signals were simultaneously recorded using disposable adhesive Ag/AgCl electrodes (H27P, Kendall-LTP, MA, USA) placed in a tripolar configuration (active–common–reference) over the tremulous forearm extensor (carpi ulnaris) and flexor (carpi radialis).

The measured signals were then amplified using isolated CED 1902 amplifiers (×10,000 for LFPs and ×1000 for EMGs), filtered at 0.5–500 Hz and digitized using CED 1401 mark II at rates between 250-1000 Hz. For the patients concerned, after a two week recovery period the electrode leads were internalised and connected to an implanted pulse generator (Medtronic KINETRA® model 7428) which was surgically inserted into the chest cavity.

2.2 Dataset description

Our entire database of recorded raw LFP signals consisted of 13 LFP tremor onset recordings from a total of eight patients – the details of which are given in Table 1. Out of the 8 patients included in the study, only two – P1 and P2 – were implanted in the GPi nucleus, while the remaining 6 received STN implants. The data chunk counts presented in the table were obtained using 2 seconds long chunks (500 samples) with 90% overlap. Onset chunks were those found in a 4 seconds region around EMG-based tremor onset (see the next section for further details). Note: Each chunk consists of collected data within a 2 seconds window.

patient ID	target	files	total length [s]	Chunk counts			
				Atrem.	Onset	Trem.	Total
P1	STN	1	60.0	114	30	146	290
P2	STN	4	147.0	253	120	325	698
P3	STN	1	60.0	101	30	159	290
P4	GPi	1	25.0	51	30	35	116
P5	STN	1	30.0	38	30	72	140
P6	GPi	2	97.0	205	60	201	466
P7	STN	2	48.5	38	60	126	224
P8	STN	1	60.0	128	30	132	290
Total		**13**	**527.6**	**928**	**390**	**1196**	**2514**

Table 1 Dataset overview. Chunks produced using 2secs windows with 90% overlap.

The maximum amount of recordings taken from a single patient was four, although the median was only one recording per patient (Table 1). This was caused mainly by the requirement for tremor onset to be present in the recording period. The total number of recordings was 13, the total length of time 527.6secs, and the average length of each recording was 40.5secs.

2.3 Data preprocessing

Firstly, to maintain a uniform frequency across recordings, all data were down-sampled to 250 Hz (the lowest sampling frequency used). A 3-30 Hz and 3-7 Hz (tremor band) Chebyshev Type II passband filter was used on the recorded LFP and EMG signals respectively. The EMG signal was then normalized and rectified. Low frequency LFP activity systematically relates to slow drift movement artefacts, while frequencies above the beta-band (30 Hz) are considered to hold little tremor-related information. Indeed this frequency range also includes abundant 50 Hz line noise.

Tremor onset was calculated for each file based on the amplitude of filtered and rectified EMG signal. The magnitude of the EMG time series value was checked against a threshold of three times the mean of the EMG magnitude in the first 5secs of the recording (known to be recorded during atremorous activity – that is LFP activity when no tremors were apparent). If an indication of high tremor frequency activity was determined at any point in time then the mean of the next 5secs of data (long enough to cover any period of small tremor-onset) was calculated to confirm the initial tremor detection. A single time of tremor onset was calculated for each patient recording. This calculated point was then used for data annotation and division of the data into into tremor and atremorous sets.

2.4 Feature extraction (feature calculation from the raw signal)

Feature extraction involves representing the raw signal in terms of a smaller set of quantities, termed features. Feature measurement from biological signals is a routine process in biomedical studies, however, correct feature selection is fundamental in order to relate signal characteristics to various biological measures such as the detection and classification of tremor in an LFP signal. Many features or feature sets exist in biomedical engineering for signals such as ECG, EEG and EMG (Ciaccio et al., 1994), whereas LFP signals taken from humans have only been readily available to researchers since the early 1990s.

In this section we consider a range of different features and explain how their characteristics are obtained from the original raw LFP data. The LFP data here is divided into two second chunks with 90% overlapping so a spatial resolution of 0.117Hz and a time resolution of 0.2secs was achieved. The Hamming window was applied to each chunk and

the data was treated as a discrete signal and passed through each feature function. Evaluation of the performance of individual features in different patients is given in section 0.

2.4.1 Time domain

Increased LFP oscillation energy is known to be related to the excitation and synchronised firing of active neurons in the motor cortex (Denker et al., 2007) and in the Parkinsonian STN (Loukas and Brown, 2004; Rivlin-Etzion et al., 2006). Furthermore, discharges of single STN neurons are often coupled to Parkinsonian tremor oscillatory activity (Kühn et al., 2005; Moran et al., 2008; Weinberger et al., 2006). Signal power is a time average of signal energy, and is useful when the energy of the signal goes to infinity, such as infinite LFP activity within the basal ganglia. Therefore, segments of signal energy are estimated from the area under the curve within the boundaries of the data chunk.

A feature termed *mag* calculates a time average of energy over a discrete signal, and can detect the presence of short attenuations in a signal, which are commonly identified as undesirable artifacts. The *mag* feature output is defined as

$$mag = \frac{1}{n}\sum_{t=1}^{n}|x(t)|^2 \tag{1}$$

where t is time, and x is the discrete LFP signal of length n.

LFP activity from the basal ganglia is a signal of infinite length (a lifetime) and so it is impossible to assert the 'true' variance of the population (all neurophysiological data). Instead a sample variance can be measured from the finite atremorous and tremorous LFP signals provided. For this an unbiased variance calculation is used to compensate for the discrepancy of the sample and population. Given that LFP signals oscillate in time, the sample variance is never exactly zero, consequently, the larger the variance, so the more variability there is in the measured sample.

The variance feature (termed *var*) is designed to simply return the variance of the given LFP signal window and it is used to analyse abnormal LFP oscillatory activity. The magnitude of the *var* feature is hypothesised to increase during periods of tremor, at which

times sporadic abnormal neuronal activity is known to develop. The population mean, μ, and variance ,σ^2, of a signal can be calculated by means of Eq. 2 and Eq. 3 respectively if data for all of the population is known. The mean being

$$\mu = \frac{1}{N}\sum_{t=1}^{N} x(t) \tag{2}$$

where μ is the population mean of the time series $x(t)$ of size N.

Meanwhile the population variance is obtained from

$$\sigma^2 = \frac{1}{N}\sum_{t=1}^{N} (x(t) - \mu)^2 \tag{3}$$

However, each patient recording is a sample taken from the entire population of neurophysiological data, so the feature, *var,* is the sample variance, given by

$$var = \frac{1}{n-1}\sum_{t=1}^{n} (x(t) - \bar{x})^2 \tag{4}$$

where $\bar{x}$ is the sample mean of the time series $x(t)$ of size n, given by

$$\bar{x} = \frac{1}{n-1}\sum_{t=1}^{n} x(t) \tag{5}$$

The zero-crossing rate (a feature name *zerox*) is arguably the simplest form of frequency analysis in the time domain. This feature crudely measures the frequency of a signal with zero mean by counting the number of times the LFP signal value crosses zero magnitude in a given time window. Consequently, higher frequency signals produce a greater zero-crossing rate and vice versa.

Quite a number of zero crossing based frequency estimation methods have traditionally been used in applications such as speech and communications (Anderson, 1982; Wiley et al., 1977), additionally a study of the zero crossing rate has also been used in biomedical engineering for EMG (Masuda et al., 1982; Skotte et al., 2005) and EEG (Chi-Hsun

Wua et al., 2011) analysis. This feature counts the number of times the LFP signal value crosses zero magnitude in a segment of LFP data, and can be expressed as

$$zerox = \sum_{t=2}^{n} \begin{cases} 1, x(t)x(t-1) = 0 \\ 0, otherwise \end{cases} \quad (6)$$

where n is the length of the segment.

The application of autocorrelation in neurophysiological signals was first used to analyse EEG signals as early as 1950 (Brazier and Casby, 1952), and despite the introduction of the FFT, the autocorrelation function is to date commonly employed to estimate statistical moments of the PSD (Derya Ubeyli, 2009; Jackson et al., 2008; Tagluk and Sezgin, 2011). Autocorrelation is useful for finding repeating patterns in a signal, determining the presence of a periodic signal which has been buried under noise, and identifying the fundamental frequency of a signal which doesn't actually contain that frequency component, but implies it with many harmonic frequencies.

Autocorrelation is simply the correlation of a discrete time series $x(t)$ against a time-shifted version of itself. The discrete autocorrelation R at time lag j for the signal $x(t)$ is defined as

$$R(j) = \sum_{t=1}^{n} (x(t) - \bar{x})(x(t-j) - \bar{x}) \quad (7)$$

where $\bar{x}$ is the sample mean.

The area under the curve between bands is calculated and used for the *ac_tremor* and *ac_beta* features, written as

$$ac\_band = \sum_{j=\beta_2}^{\beta_1} |R(j)| \quad (8)$$

where β_1 and β_2 are boundaries of the frequency band in units of lags, given by

$$\beta_k = \frac{n}{f_k} \tag{9}$$

In which n is the length of the signal and f_k is the pseudo frequency in Hz.

2.4.2 Information theory

All the features presented thus far share a common goal; they are all used to try to differentiate information in the LFP signal between the two main Parkinsonian tremor relationships (tremor and atremorous). The direct existence of Parkinsonian tremor relationships can however be further analysed by means of information theory. Central to this theory is the concept of entropy, which can be roughly defined as a measure of the uncertainty of a signal. A known example of a Probability Density Function (PDF) on a set of real numbers is the Gaussian distribution or normal distribution, and this can be used to describe synaptic potential amplitudes.

Because the LFP signals collected are not of Gaussian distribution (each patient recording failed the one-sample Kolmogorov Smirnov test at $p < 0.05$), the entropy is calculated using five different PDFs: i) A PDF derived from a histogram of the entire tremor-onset signal (this feature is named *entropy_entire*). ii) A PDF derived from a histogram of the atremorous LFP signal of a patient recording makes the feature *entropy_atrem*. iii) A PDF derived from a histogram of the tremor LFP signal of the patient recording makes the feature *entropy_trem.* vi) A PDF derived from a histogram of the windowed LFP data termed *entropy_win*. v) Finally, despite the failed Kolmogorov Smirnov test a normal PDF is created using the mean and standard deviation of the entire tremor-onset signal, this feature is named *entropy_norm*. The feature output is given by,

$$entropy\_(p_k) = -\sum_{t=1}^{n} p_k x(t) \log p_k x(t) \tag{10}$$

where k is the data used to calculate the PDF $p$and this therefore defines the entropy feature.

2.4.3 Frequency domain

Pre-defined frequency bands classifying activity in the human brain can be used to determine its current functional state, and changes in the spectral properties of LFP activity recorded from the basal ganglia of a Parkinsonian patient are also known to correspond to tremorous movement (Amtage et al., 2008). The spectrum activity of the basal ganglia can be classified into four groups or bands: tremor (3.5-5.5 Hz), theta (5.5-8 Hz), alpha (8-12 Hz), and beta (12-30 Hz). The gamma band (30-100 Hz) was contaminated with heavy 50Hz noise and was thus removed in the pre-processing stage, as described earlier in section 2.3.

The Fourier transform is a function that decomposes a signal into its constituent frequencies, and can be obtained by

$$F(u) = \frac{1}{n}\sum_{t=1}^{n} x(t)e^{-i2\pi ut/n} \tag{11}$$

The *freq_band* feature looks at the frequency properties of the signal and calculates the magnitude of the PSD within the boundaries of alternate frequency bands, here

$$freq\_band = \sum_{u=\delta_1}^{\delta_2} |f(u)|^2 \tag{12}$$

where $f(u)$ is the Fourier transform of $x(t)$, and δ is the boundary of the frequency band.Figure 1: Spectral comparison of averaged atremorous and tremorous LFP signals.

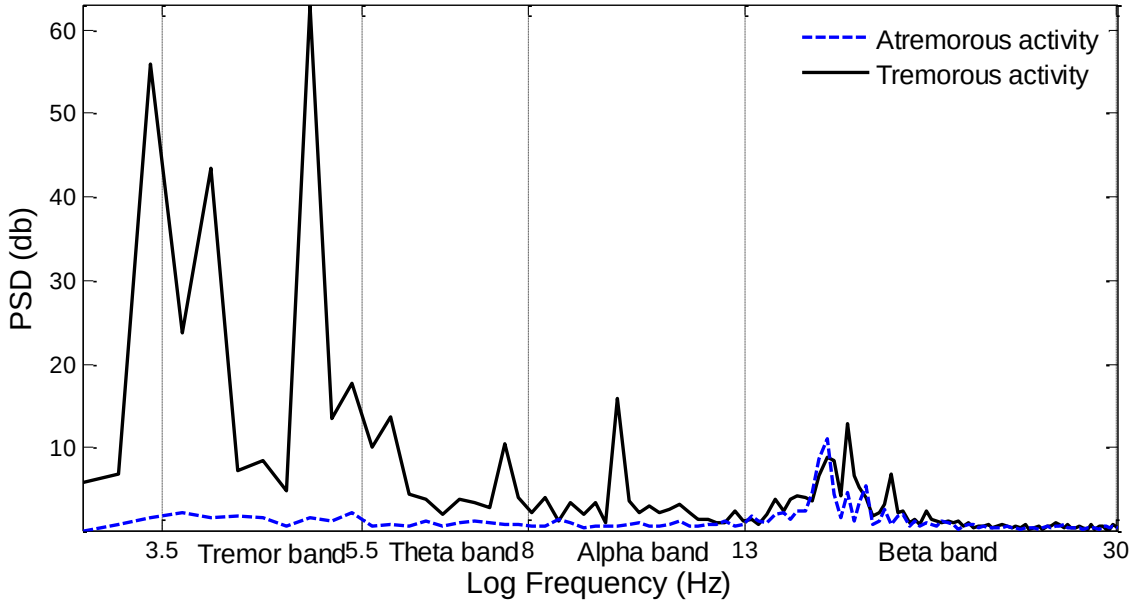

Figure 2: Spectral comparison of averaged atremorous and tremorous LFP signals.

The tremor frequency band used in this feature is set as 3.5 – 5.5 Hz. This band was selected in particular because it matches the appearance of increased PSD during episodes of tremor, as can be seen in Figure 1: Spectral comparison of averaged atremorous and tremorous LFP signals. The theta-band (5.5 – 8 Hz) is though closely related to the tremor-band, and may capture some outliners. In such an event the PSD mean from tremor periods is expected to follow closely to that of the tremor-band and be slightly higher than from atremorous periods, albeit not as significant. On the other hand, the alpha-band (8 – 12 Hz) has not been reported in previous research to have a significant association with PD tremor.

It is noticeable that in Figure 1. we have selected a window 3.5-5.5 Hz, yet it can be seen that there is significant activity below this frequency band. We have selected the frequency range in question because of the desire to select one range to cover the published tremor frequency range (Hutchison et al., 1997; Lemstra et al., 1999; Liu et al., 2002; Magarinos-Ascone et al., 2000; Wang et al., 2007). We believe that it will make an interesting future study to consider a two window method, splitting the tremor range between the to two frequency bands. An option to build a robust tremor-detecting feature could also involve searching for a maximum (tremor-frequency peak) in the tremor range. However, this inspection would require further evaluation of the tremor-frequency signal in the LFP signals, which can be verified in future studies.

2.4.4 Continuous Wavelet Transform

The Continuous Wavelet Transform (CWT) is similar to the time-frequency method of the Short Time Fourier Transform (STFT), but rather a time-scale analysis is performed. The compromise between time and frequency information from an STFT can be practicable, nonetheless a fixed length window is used throughout the process. Nonstationary signals like LFPs can often require a variable-sized window approach which can enhance either time or frequency information.

The length of the window determines either precise low-frequency information using long segments, or high-frequency information using shorter segments. Unlike the Fourier transform, which breaks up a signal into sinusoids of various frequencies, the CWT decomposes a signal using a family of 'wavelets' varying in scale to collect shifted and scaled information. An estimation of frequency, called the pseudo-frequency, can be calculated from the scale-time signal using Equation 13, and this is employed to measure the activity in the tremor- and beta-bands.

$$a = \frac{F_s F_c}{F_a}, \tag{13}$$

where, a is the scale, F_s is the sampling frequency, F_c is the centre frequency of the wavelet, and Fa is the pseudo-frequency[1].

The usual notation of the Continuous Wavelet Transform (CWT) is

$$CWT_x(a,\tau) = \frac{1}{\sqrt{a}} \int x(t) \varphi^* \left(\frac{t-\tau}{a}\right) \mathrm{d}t \tag{14}$$

In which φ is the basic wavelet function or the so-called *mother wavelet*, a is the scale factor and τ is the translation in time.

In the CWT feature we chose the Shannon wavelet as the mother wavelet. A Shannon complex wavelet is symmetrical in shape and can compute the complex

[1] The pseudo-frequency is only an approximation of the frequency because the centre frequency is an approximation of the dominant frequency in the wavelet oscillations.

continuous wavelet transform when given two adjustable parameters, the bandwidth and centre frequency. Using a bandwidth of 0.2 and centre frequency of 2 Hz, a good temporal-spectral resolution is achieved for analysing the tremor frequency (3.5-5.5 Hz) and the beta frequency (12-30 Hz) in LFP signals from the patient database. This feature is named *wav_#*, where *#* is the frequency band (either *tremor* or *beta*).

2.4.5 Discrete Wavelet Transform

The Discrete Wavelet Transform (DWT) is an extension of the CWT and is a generalization of wavelet decomposition that offers a rich range of possibilities for signal analysis. The transform decomposes a signal into an approximation and a detail. The approximation or detail itself is then split into a second-level approximation and detail, and the process is repeated until the desired level of decomposition is reached, resulting in a complete binary tree of all possible decompositions. The approximation of a signal is obtained by convolving the signal with a low-pass filter and with a high-pass filter for detail decomposition.

The DWT feature termed *wavdetail* returns the detail wavelet decomposition at the 5th level of the approximation. After which frequencies in the high beta-band are suppressed; leaving the tremor, theta, alpha, and low beta-band frequencies in the signal.

The DWT of a signal $x(t)$ is calculated by passing it through a series of filters:

$$DWT_{high}(u) = \sum_{t=1}^{N} x(t)g(t-u) \tag{16}$$

$$DWT_{low}(u) = \sum_{t=1}^{N} x(t)h(t-u) \tag{17}$$

where g is a low-pass filter which returns approximation coefficients, and h is a high pass filter which returns detail coefficients.

After each DWT transform (or decomposition) the coefficients are down-sampled by two, since half the frequencies of the signal have been removed in the process. The feature *wavdetail* is the sum of the squared magnitude of the 5th detail of the signal $x(t)$, written as

$$wavdetail = \sum_{u=1}^{n/2^5} \left| DWT_{high}(u_4) \right| \tag{18}$$

where u_4 is the 4th detail decomposition of $x(t)$.

2.5 Neural network multi-feature classification

In a multi-feature classification, the discriminative power of the classifier is based on a set of observed or calculated characteristics of the training examples – the features. The main advantage of this approach is that even features showing low discriminative power when observed individually (a single-feature classification) can potentially achieve better classification performance when combined together. This is based on the multi-dimensional information, contained in the whole features set, assuming low inter-feature correlation.

In this study, we assumed that the tremor-related changes in the LFP signals were not bound exclusively to one type of signal transformation – such as frequency spectrum – but that these changes could be observed from different signal properties. To accomplish this, features based on different properties of the LFP signals were combined in a single classifier, which should lead to the utilization of more tremor-related information.

2.5.1 Feature selection

To design a classification system with good performance, a set of highly relevant features is necessary. Even though the features calculated according to the description in section 2.4 were designed to capture observed changes in the LFP signals, their actual classification power for the problem considered was unknown until they were applied to the data in question.

To evaluate the tremor classification power of individual features, a relative information gain metric was adopted. The relative information gain value represents the relative drop in entropy of the system in the case when a particular feature's value was

known. In the simplified case of two random variables, the relative information gain (denoted by G) can be represented by the formula given in (19):

$$G(X) = \frac{H(Y) - H(Y \mid X)}{H(Y)} \tag{19}$$

Where G(X) is the relative information gain of the feature X, H(Y) is the entropy of attribute Y and H(Y|X) is the conditional entropy of feature Y, given that the value of X is known.

Before the features were entered into the input layer of the neural network model, the relative information gain was calculated for each of them. Features with G<0.1 were considered to be suitably insignificant and were, on this basis, excluded from further processing. Results of the feature evaluation and selection are described in section 0.

2.5.2 Neural network classifier

To distinguish tremor and atremorous data based on the feature values, an artificial neural network (or commonly referred to merely as neural network – NN) classifier was used in this study. NN models have universal nonlinear modelling and classification capabilities which together with high noise tolerance makes them suitable for a wide array of diagnostic machine learning tasks (Hornik et al., 1989; Reggia et al., 1993). Due to their listed versatile properties, NN models have been used for the processing of various biomedical signals since the early 1990's (Reggia et al., 1993) and have become quite commonly applied as an analysis technique for biomedical signals such as EEG in the last few years (Ubeyli, 2008), [39].

In this study, a feed-forward neural network classifier with one hidden layer was used and trained on the training data subset. The training process was limited to 200 learning cycles in order to avoid model overfitting, which was apparent at higher training cycle counts. The input to the classifier was formed by feature values, calculated on individual 2secs chunks. The number of hidden layer neurons (neurons in the middle – not input or output layer) was 10, chosen according to the best performance achieved at this network setup. The number of input layer neurons was adjusted in each cycle according to the actual number of attributes after feature selection.

2.6 Machine learning procedure

Conventionally a multi-feature classification process consists of building a feature set, classifier training and then evaluating the overall model's performance on unseen data. This section describes all the aforementioned steps including modifications, done to accommodate the specifics of the tremor detection task.

Feature extraction from raw data was performed in MathWorks MATLAB environment, while the feature selection and classifier evaluation process was carried out in Rapid-i RapidMiner data mining software.

2.6.1 Global and patient-specific classification

Before the classification procedure could be embarked upon, consideration had to be given to the problem of handling data from different patients. A basic supposition, necessary for the multi-feature classification system to be feasible at all, is that different PD patients not only share similar characteristics in their brain activity during both tremor and atremorous periods but also exhibit similar characteristics during periods of change from one state to the other.

On this assumption it is sensible to suppose that the changes in different patients can be described by similar features (e.g. changes in signal power, changes in frequency spectrum etc.). However, it is very likely that LFP signal properties actually vary dependant on many factors, including individual patient factors such as sex, age, PD progression and the exact positioning of the stimulation electrodes within the target structure. Thus, the classification system has to be designed in an attempt to address these issues properly.

Generally, there are two possible approaches to the classification of such signals: a) create a model on a per-patient basis, i.e. the model is trained specifically for each patient b) train a global universal classifier, for the detection of any patient's LFP signals. The latter approach puts much higher requirements on the consistency of tremor-related changes across different patients. Despite this, we considered/hypothesized such a system to be feasible and selected a general classifier as the approach to be used in this study.

In a sense we were thinking about the long term aspects of the end product from our research. Potential advantages being an easier setup procedure with no need for physician

training together with versatility of use. Moreover, a design process based on such a system can itself bring much new information about patient-dependent changes.

2.6.2 Classifier training and validation

A common measure of classifier quality is classification performance, given typically by accuracy – the ratio of correctly classified examples to the number of all examples – or error (1 - accuracy). To estimate classification performance of the trained model properly, the examples, presented to the model in the testing period have to be unseen by the classifier during training. This approach, contrary to performance on the testing data, gives a good estimate of the generalization properties of the classifier.

The simplest method to calculate performance estimate is split validation, where data is randomly split into two data sets: the training and testing set. The split operation assumes complete separation and independence between the training and testing sets. Due to inter-chunk dependencies, caused by the high overlap between different chunks, this technique was inapplicable to the presented problem. The dependencies were verified by a test in which the data was divided randomly into training and testing sets in the ratio 7:3 and the testing accuracy reached up to 99.75% as opposed to much higher error rates seen at different dataset splitting methods.

To ensure separated training and testing data, the data splitting method used was based on an iterative per-patient approach: in each cycle, data from one of the patients was withheld for testing and the whole training process - feature selection and model training – was performed on the remaining data. The process was repeated with each patient in the position of testing subject. Two accuracy estimates were calculated: per-patient accuracy, and overall accuracy, calculated from the total number of erroneously classified chunks. Onset chunks were left out from the training set, whereas the test set comprised all data of the testing patient, including onset chunks and one to several recordings. The overall process diagram is shown in Figure 3.

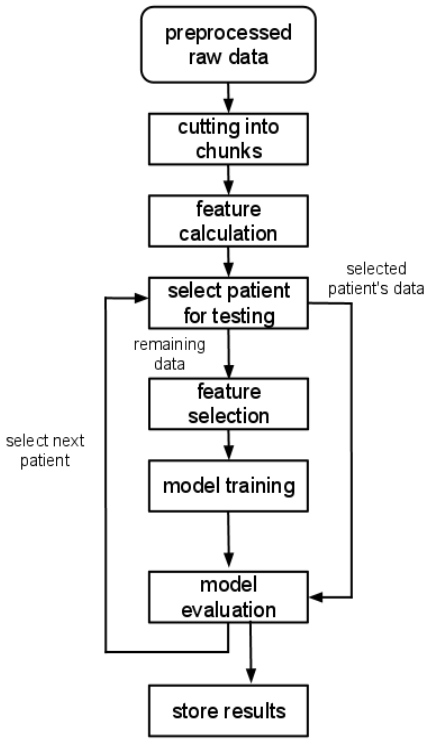

Figure 3: Diagram of the leave patient out process

Apart from avoiding problems based on inter-chunk dependencies, this approach also provides a good idea of how well the system could work in real deployment. In such a scenario, the detection algorithm would be designed and tested on a data sample similar to that used in this study, with no need for patient-specific parameter tuning or other adjustments.

3 Results and discussion

In this section we present results on our analysis of the features selected, on our testing of the accuracy of the proposed classification system in terms of its performance and the use of an in silico model to approach the possibility of real-time analysis by this means. It is worth pointing out that, in each case, the system employed was trained up on data from all the other patients in the study before being tested on each individual patient – the system therefore had not actually seen any data from the patient on which it was due to make its analysis.

As will be seen, the study provided a mixed bag of results. In some cases (for some patients) the results were exceptionally good, much better than we could have hoped for apriori. Such results indicate clearly that the approach taken can work very well. On the other hand, for some patients the results were surprisingly poor. This leads one to believe that the approach taken here is merely providing part of an overall, applicable solution.

3.1 Feature evaluation

According to the procedures described in section 2.5.1, the relative information gain was calculated (minimum = 0.0, maximum = 1.0) for each feature on each patient's data. Chunks from the onset period were excluded from this calculation. In this way, the performance of each feature could be evaluated. The comparative results from each of the different features are presented in Table 2 in a relatively ordered fashion**.**

Patient	**P1**	**P2**	**P3**	**P4**	**P5**	**P6**	**P7**	**P8**	**mean**	**std**
freq_theta	0.69	0.65	0.93	0.97	0.93	0.83	0.49	0.07	**0.70**	**0.27**
wavdetail	0.48	0.61	0.91	0.97	0.93	0.98	0.55	0.04	**0.68**	**0.29**
freq_trem	0.48	0.55	0.96	0.97	0.93	0.74	0.53	0.11	**0.66**	**0.27**
var	0.57	0.26	0.96	0.97	0.93	1.00	0.49	0.06	**0.66**	**0.32**
entropy_norm	0.54	0.27	0.96	0.97	0.93	1.00	0.49	0.04	**0.65**	**0.33**
wav_tremor	0.55	0.26	0.96	0.97	0.93	0.70	0.61	0.12	**0.64**	**0.28**
freq_alpha	0.42	0.10	0.96	0.97	0.93	1.00	0.49	0.14	**0.63**	**0.34**
entropy_atrem	0.52	0.17	0.96	0.97	0.93	0.58	0.78	0.09	**0.63**	**0.31**
entropy_entire	0.50	0.29	0.96	0.97	0.93	0.73	0.29	0.07	**0.59**	**0.31**
wav_beta	0.09	0.06	0.96	0.97	0.93	1.00	0.24	0.20	**0.56**	**0.39**
freq_beta	0.08	0.01	0.88	0.97	0.93	0.46	0.28	0.24	**0.48**	**0.35**
zerox	0.46	0.27	0.93	0.21	0.93	0.13	0.16	0.06	**0.39**	**0.31**
ac_tremor	0.27	0.07	0.75	0.14	0.93	0.24	0.20	0.03	**0.33**	**0.29**
ac_beta	0.58	0.09	0.32	0.05	0.83	0.12	0.21	0.04	**0.28**	**0.25**
entropy_trem	0.11	0.10	0.62	0.36	0.22	0.38	0.09	0.09	**0.24**	**0.17**
entropy_window	0.13	0.04	0.28	0.07	0.37	0.07	0.09	0.03	**0.14**	**0.11**

Table 2 Information gain of individual features in different patients

As seen from the values in the table, despite the fact that the performance of all features varies substantially between patients, the features can be categorized according to

overall performance across the set. The first five features in the table – *freq_theta* to *entropy_norm* – are best rated according to their IG value and seem to be the most stable ones according to their top (or at least high) ranking in most patients. The rest of the features showed either mixed performance (e.g. *wav_beta*, *freq_beta*, *entropy_entire*) or poor performance overall (*entropy_trem*, *entropy_window*).

What is not perhaps so clear to see from Table 2 is that patients' results seemed to cluster and can be divided into the following three groups, based on common IG values: a) patients with IG close to one in most features. This includes patients: P3, P4, P5, P6. Tremor activity in these patients should be possible to classify by means of individual features or small feature groups. b) Patients with moderate IG values. This includes patients P1, P2 and P7. c) Patient P8 with extremely low IG values in all features. Classification of this patient, based on the calculated features seems unfeasible.

3.2 In silico model

Due to the time needed to record a reasonable amount of data and the fact that the long perioperative period, in which the data can be collected, is only a few days long, we were unable to evaluate performance of the system in day-to-day, living conditions. Thus, In order to provide an easy to assess performance test of the whole multi-feature neural network system, we carried out an in-silico test. To split the training and testing data in a manner comparable to real deployment, we evaluated the system using the leave-one patient-out method, where one patient's data is held out for testing and the NN model is trained on the remaining part of the dataset, which means that no data from the testing patient were seen by the classifier prior to testing. The evaluation system was described in greater detail earlier in section 2.6.

Once the data was fully classified – each patient's data having been in the position of a testing subject – all chunks were labeled by the classifier and the performance of the system could be evaluated. To show the results from different perspectives, we have provided here two different types of performance evaluation: common classification accuracy measures and temporal output figures, which will be discussed further, later on.

In Table 3 the figures indicate test classification accuracy, calculated as a percentage of correctly classified chunks for the patient in the position of testing subject. Percentages are given separately for atremorous and tremorous chunks. The overall accuracy is calculated from the total number of correctly classified chunks. Onset chunks were not considered in the accuracy calculation.

patient	**P1**	**P2**	**P3**	**P4**	**P5**	**P6**	**P7**	**P8**	**total**
target	STN	STN	STN	GPi	STN	GPi	STN	STN	
atrem	68,4	94,1	100	100	100	100	71,1	18	**83,1**
trem	92,5	59,4	74,8	100	98,6	71,9	81,8	99,2	**78,1**
total	**81,9**	**74,6**	**90,4**	**100**	**99,1**	**86,2**	**79,3**	**59,2**	**80,4**

Table 3 Classification accuracy in individual patients: tremorous, atremorous chunks and overall results. Accuracies calculated from actual numbers of correctly classified chunks - onset chunks not considered.

As seen from the table, quite large differences in classification accuracy are present in the different patients. In two patients – *P4* and *P5* – the classification accuracy reached almost 100% for both tremorous and atremorous activity, which is outstanding, considering that only data from the other patients were used for classifier training. In another patient group however, including *P6*, *P3* and *P2*, the classification of atremorous data was very accurate, whilst the tremor detecting capability was low. The completely opposite situation can though be seen in *P8*, where tremorous data was classified with 99.2% accuracy, while atremorous data was hardly recognised with only 19%, which means in reality that most chunks were classified as tremorous, even when they were not. Regarding different stimulation – and thus recording – targets, it can be noted that the two patients with electrodes implanted in the GPi were among the patients with the best classification results. However, due to the low number of test examples, no strong conclusion about suitability of either nucleus for tremor detection can be drawn.

A more easily readable representation of the classification results may be obtained in terms of visualization of the classifier output, compared to actual LFP signals and forearm EMG activity. Selected plots, showing these three quantities for three different patients are shown in Figure 3.

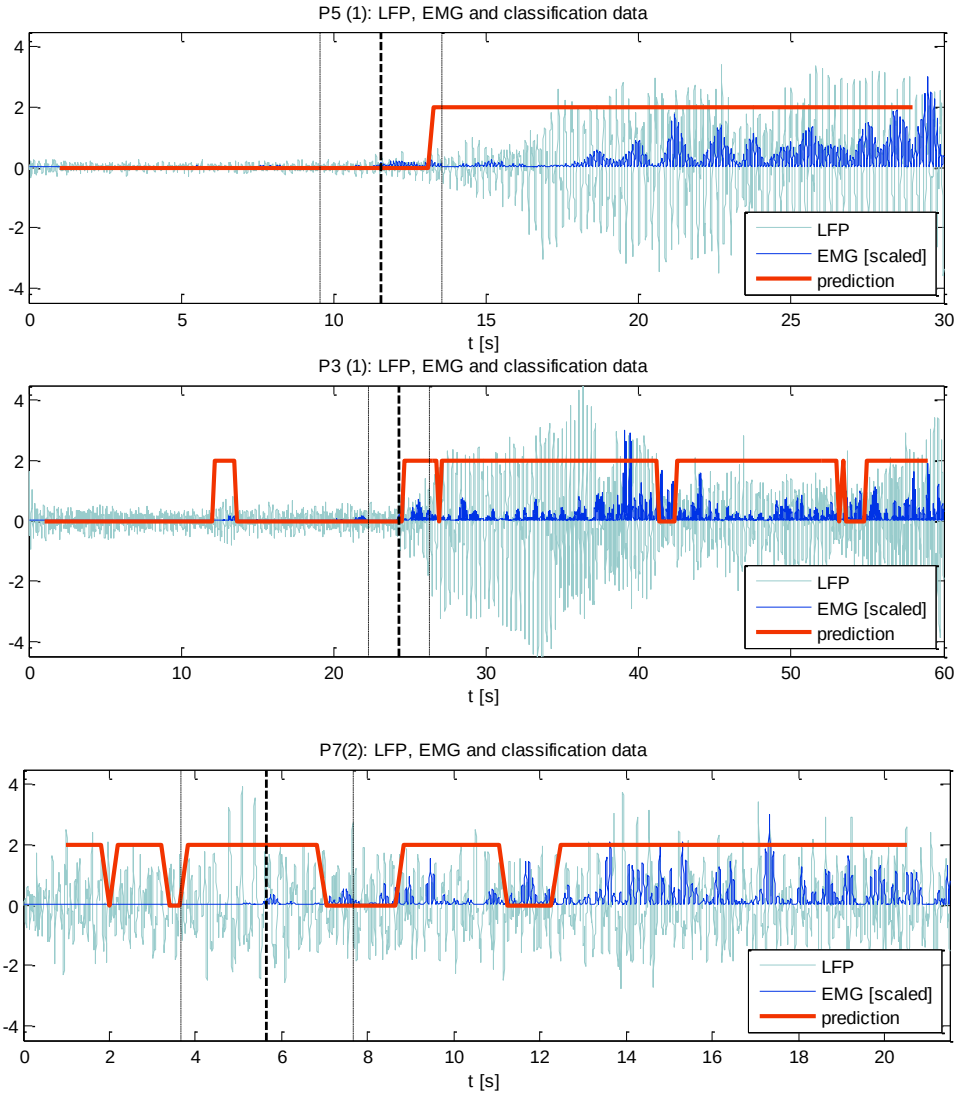

Figure 4: Tremor prediction on three patients, unseen previously by the classifier. The original LFP signal is shown along with flexor EMG activity and model output.

The classifier output and EMG signal were scaled to match common amplitudes of the LFP signals and be easily readable in the plots. Outputs of three patients were selected, representing very good, medium and poor performance respectively. The plots can be matched to corresponding accuracy values in Table 3. to gain an overall view of system performance. Unlike in the case of the calculation of accuracy, classified tremor onset chunks were included in these plots to maintain continuity of the system output throughout each file. Discussion of the experimental results is given in the following section.

3.3 Discussion of the results

In this paper we inspected a hypothesis that the onset of Parkinsonian tremor could be detected directly from the stimulation electrodes and used for on-demand stimulation. Moreover, we suggested that a single parameter setting could be sufficient and tested this assumption on a set of 8 patients. This section aims at commenting on and a discussion of possible causes that lead to the mixed classification results.

The results presented in the previous section show very mixed classification performance in different patients. Comparing classification accuracies in

patient	**P1**	**P2**	**P3**	**P4**	**P5**	**P6**	**P7**	**P8**	**total**
target	STN	STN	STN	GPi	STN	GPi	STN	STN	
atrem	68,4	94,1	100	100	100	100	71,1	18	**83,1**
trem	92,5	59,4	74,8	100	98,6	71,9	81,8	99,2	**78,1**
total	**81,9**	**74,6**	**90,4**	**100**	**99,1**	**86,2**	**79,3**	**59,2**	**80,4**

Table 3 to feature information gain values in Table 2, a link between poor performance of the best features and poor classification accuracy seems obvious (a similar link can be seen in 'well performing patients', too). This was probably also the reason for the poor classification accuracy of patient 8: for example features, such as *freq_theta* or *wavdetail*, very strong in other patients, showed extremely poor classification power with respect to tremor. Drawing a conclusion about the link between feature performance and classification accuracy seems sensible, however the reasons for poor feature power in some patients are unclear and may be connected with unknown underlying structures in the patient set.

High model accuracy in some patients, together with the error estimation procedure with model training and testing on separate patients, suggests similar tremor-correlated signal properties across the whole dataset. On the other hand, the low system accuracy in some other patients suggests these tremor-bound properties are shared by only a subgroup of all patients. Unfortunately, the size of the dataset does not allow for drawing conclusions about different patient subgroups, based on the tremor-related properties of LFP signals.

Another effect that could have contributed to the mixed results of different patients might be the method of specification of tremor onset from EMG data. Possible patient variability in time shift between the outbreak of tremor-related changes in the LFP signals and tremor onset detected in the EMG activity may shift the classification accuracy significantly. This could be one explanation for the extremely poor specificity in patient P8: the results might be improved if the EMG tremor onset were marked earlier. To achieve accurate tremor detection, manually marked tremor onset, based on observation of the patient would be needed.

This also applies to classification accuracy based on LFP from different nuclei: even though the classification accuracy for both patients with GPi implants was relatively high, the lack of data does not allow for more general conclusions. The small amount of data was the reason why treating all available patients as one coherent group was the only option for unbiased error estimation and was therefore chosen in this study.

Unlike epileptic pre-seizure periods, Subthalamic nuclei in the Parkinsonian brain are thought to display tremor synchronization activity only seconds (rather than minutes) before severe muscle tremor starts (Brown, 2003; Wang et al., 2007).This places greater responsibility and urgency on the classification algorithm. In this study, tremor period annotation was calculated from filtered normalized forearm EMG (described above). Even though the calculation was designed to be patient-independent, the precision of such a detection procedure can only be accurate to a certain extent. Possible variance of the delay between outbreak of tremor synchronization activity in the LFP signals and actual muscular tremor may be the source of improper annotation and thus increased classification error.

In the tremor detection task, sensitivity is of primary importance, as it represents the retention of the permanent beneficial effect of the stimulator. Specificity in this case represents battery saving capabilities for the system and is therefore not as important. Thus, an ideal classification system should be tuned for maximum possible sensitivity to retain an equivalent effect to that of full-time stimulation. The NN model, used in this study, does not allow favouring one of the classes and hence a more detailed look at sensitivity will be part of further work.

The study in this paper has focused strictly on analyzing and detecting tremor periods. The basis for this being a desire to understand more fully the links between tremor onset and LFP signals. This is a clear step towards accurately predicting tremor onset such that a signal can be employed as an adaptive trigger to fire the stimulator as part of a feedback loop before tremors actually occur. Studies are also ongoing into tremor prediction (Pan et al., 2012; Wu et al., 2010) the desire here however is to provide a stronger base for further research along these lines.Despite the limitations caused by the relatively small amount of data, the accuracy estimation on unseen patients which was implemented in this study should provide unbiased results. Moreover, the results show that a universal classifier without the need of parameter tuning for specific patient is feasible with satisfactory results at least for a subgroup of patients. The requirements that have to be fulfilled for such a detector to be broadly applicable remain among the research questions yet to be answered.

4 Conclusions

A system for online detection of Parkinson disease tremor, based on LFP signal features of different kinds, was proposed in this study. A global classifier without the necessity of parameter-tuning was developed and tested. Despite the fact that a patient non-specific model was trained, very good results were obtained for four out of eight patients, supporting the feasibility of the multi-feature NN approach in tremor detection for some patients at least. The performance of the system on unseen patients showed that at least a subgroup of the patients could benefit from the system, if and when it was implemented in a stimulator device.

To draw more general conclusions about performance – especially stability and robustness – of the system, a much wider dataset, including data from different positions and situations in different individuals will be necessary. Larger amount of data could also provide a basis for the further evaluation of individual feature properties, possible patient types or differences in classification accuracy between different targets. This is the subject of ongoing research.

One final comment is that it may well be the case that patients with PD can be grouped in terms of the LFP activity witnessed in atremorous, tremorous and onset time periods. Certainly from our limited studies thus far – both reported on here and otherwise (Burgess et al., 2010) – this would appear to be a natural conclusion. Such a classification would indeed dramatically improve the recognition accuracy if features selected and network training were restricted to patients within each group. A question underlying this conclusion however is whether or not the existence of such groups can be associated with underlying neurological relationships.

5 Acknowledgements

This work has been supported by Czech Science Foundation research program 309/09/1145 and by Grant Agency of the Czech Technical University in Prague; grant No. SGS10/279/OHK3/3T/13.

6 References

Amtage F, Henschel K, Schelter B, Vesper J, Timmer J, Lucking CH, Hellwig B. Tremor-correlated neuronal activity in the subthalamic nucleus of Parkinsonian patients. Neuroscience Letters, 2008; 442: 195-9.

Anderson JC. Improved zerocrossing method enhances digital speech. Everything Designers Need, 1982; 2: 171-4.

Baker MG, Graham L. The journey: Parkinson's disease. BMJ, 2004; 329: 611-4.

Brazier MA, Casby JU. Crosscorrelation and autocorrelation studies of electroencephalographic potentials. Electroencephalography and Clinical Neurophysiology, 1952; 4: 201-11.

Brown P. Oscillatory nature of human basal ganglia activity: relationship to the pathophysiology of Parkinson's disease. Mov Disord, 2003; 18: 357-63.

Burgess JG, Warwick K, Ruiz V, Gasson MN, Aziz TZ, Brittain JS, Stein J. Identifying tremor-related characteristics of basal ganglia nuclei during movement in the Parkinsonian patient. Parkinsonism & related disorders, 2010; 16: 671-5.

Carr J. Tremor in Parkinson's disease. Parkinsonism Relat Disord, 2002; 8: 223-34.

Ciaccio EJ, Dunn SM, Akay M. Biosignal Pattern-Recognition and Interpretation Systems. Ieee Eng Med Biol, 1994; 13: 269-&.

Denker M, Roux S, Timme M, Riehle A, Grün S. Phase synchronization between LFP and spiking activity in motor cortex during movement preparation Neurocomputing, 2007; 70: 2096-101.

Derya Ubeyli E. Statistics over features: EEG signals analysis. Computers in Biology and Medicine, 2009; 39: 733-41.

Deuschl G, Bain P, Brin M. Consensus statement of the Movement Disorder Society on Tremor. Ad Hoc Scientific Committee. Mov Disord, 1998; 13: 2-23.

Hammond C, Bergman H, Brown P. Pathological synchronization in Parkinson's disease: networks, models and treatments. Trends Neurosci, 2007; 30: 357-64.

Hornik K, Stinchcombe M, White H. Multilayer Feedforward Networks Are Universal Approximators. Neural Networks, 1989; 2: 359-66.

Hutchison WD, Lozano AM, Tasker RR, Lang AE, Dostrovsky JO. Identification and characterization of neurons with tremor-frequency activity in human globus pallidus. Experimental brain research. Experimentelle Hirnforschung. Experimentation cerebrale, 1997; 113: 557-63.

Chi-Hsun Wua, Hsiang-Chih Chang, Po-Lei Leea, Kuen-Shing Li, Jyun-Jie Sie, Sun C-W, Chia-Yen Yang, Po-Hung Li, Hua-Ting Deng, Shyu K-K. Frequency recognition in an SSVEP-based brain computer interface using empirical mode decomposition and refined generalized zero-crossing. Journal of neuroscience methods, 2011; 196: 170-81.

Jackson J, Young CK, Hu B, Bland BH. High frequency stimulation of the posterior hypothalamic nucleus restores movement and reinstates hippocampal-striatal theta coherence following haloperidol-induced catalepsy. Experimental Neurology, 2008; 213: 210-9.

Kuhn AA, Kempf F, Brucke C, Gaynor Doyle L, Martinez-Torres I, Pogosyan A, Trottenberg T, Kupsch A, Schneider GH, Hariz MI, Vandenberghe W, Nuttin B, Brown P. High-frequency stimulation of the subthalamic nucleus suppresses oscillatory beta activity in patients with Parkinson's disease in parallel with improvement in motor performance. The Journal of neuroscience : the official journal of the Society for Neuroscience, 2008; 28: 6165-73.

Kühn AA, Trottenberg T, Kivi A, Kupsch A, Schneider GH, Brown P. The relationship between local field potential and neuronal discharge in the subthalamic nucleus of patients with Parkinson's disease. Experimental Neurology, 2005; 194: 212-20.

Lemstra AW, Verhagen Metman L, Lee JI, Dougherty PM, Lenz FA. Tremor-frequency (3-6 Hz) activity in the sensorimotor arm representation of the internal segment of the globus pallidus in patients with Parkinson's disease. Neuroscience Letters, 1999; 267: 129-32.

Levy R, Hutchison WD, Lozano AM, Dostrovsky JO. Synchronized neuronal discharge in the basal ganglia of parkinsonian patients is limited to oscillatory activity. The Journal of neuroscience : the official journal of the Society for Neuroscience, 2002; 22: 2855-61.

Liu X, Ford-Dunn HL, Hayward GN, Nandi D, Miall RC, Aziz TZ, Stein JF. The oscillatory activity in the Parkinsonian subthalamic nucleus investigated using the macro-electrodes for deep brain stimulation. Clin Neurophysiol, 2002; 113: 1667-72.

Loukas C, Brown P. Online prediction of self-paced hand-movements from subthalamic activity using neural networks in Parkinson's disease Journal of neuroscience methods, 2004; 137: 193-205.

Magarinos-Ascone CM, Figueiras-Mendez R, Riva-Meana C, Cordoba-Fernandez A. Subthalamic neuron activity related to tremor and movement in Parkinson's disease. The European journal of neuroscience, 2000; 12: 2597-607.

Marceglia S, Fiorio M, Foffani G, Mrakic-Sposta S, Tiriticco M, Locatelli M, Caputo E, Tinazzi M, Priori A. Modulation of beta oscillations in the subthalamic area during action observation in Parkinson's disease. Neuroscience, 2009; 161: 1027-36.

Marsden JF, Ashby P, Limousin-Dowsey P, Rothwell JC, Brown P. Coherence between cerebellar thalamus, cortex and muscle in man - Cerebellar thalamus interactions. Brain : a journal of neurology, 2000; 123: 1459-70.

Marsden JF, Limousin-Dowsey P, Ashby P, Pollak P, Brown P. Subthalamic nucleus, sensorimotor cortex and muscle interrelationships in Parkinson's disease. Brain : a journal of neurology, 2001; 124: 378-88.

Masuda T, Miyano H, Sadoyama T. The measurement of muscle fiber conduction velocity using a gradient threshold zero-crossing method. IEEE Transactions on Biomedical Engineering, 1982; 29: 673-8.

Moran A, Bergman H, Israel Z, Bar-Gad I. Subthalamic nucleus functional organization revealed by parkinsonian neuronal oscillations and synchrony. Brain, 2008; 131: 3395-409.

Morrison S, Kerr G, Newell KM, Silburn PA. Differential time- and frequency-dependent structure of postural sway and finger tremor in Parkinson's disease. Neurosci Lett, 2008; 443: 123-8.

Pan S, Iplikci S, Warwick K, Aziz TZ. Parkinson's Disease tremor classification – A comparison between Support Vector Machines and neural networks. Expert Syst Appl, 2012; 39: 10764-71.

Rajput AH, Birdi S. Epidemiology of Parkinson's disease. Parkinsonism Relat Disord, 1997; 3: 175-86.

Ray NJ, Jenkinson N, Brittain J, Holland P, Joint C, Nandi D, Bain PG, Yousif N, Green A, Stein JS, Aziz TZ. The role of the subthalamic nucleus in response inhibition: evidence from deep brain stimulation for Parkinson's disease. Neuropsychologia, 2009a; 47: 2828-34.

Ray NJ, Jenkinson N, Kringelbach ML, Hansen PC, Pereira EA, Brittain JS, Holland P, Holliday IE, Owen S, Stein J, Aziz T. Abnormal thalamocortical dynamics may be altered by deep brain stimulation: using magnetoencephalography to study phantom limb pain. Journal of clinical neuroscience : official journal of the Neurosurgical Society of Australasia, 2009b; 16: 32-6.

Reggia JA, Peng Y, Tuhrim S. A Connectionist Approach to Diagnostic Problem-Solving Using Causal Networks. Inform Sciences, 1993; 70: 27-48.

Rivlin-Etzion M, Marmor O, Heimer G, Raz A, Nini A, Bergman H. Basal ganglia oscillations and pathophysiology of movement disorders. Current Opinion in Neurobiology, 2006; 16: 629-37.

Rodriguez MC, Guridi OJ, Alvarez L, Mewes K, Macias R, Vitek J, DeLong MR, Obeso JA. The subthalamic nucleus and tremor in Parkinson's disease. Mov Disord, 1998; 13 Suppl 3: 111-8.

Skotte J, Hjortskov N, Essendrop M, Schibye B, Fallentin N. Short latency stretch reflex in human lumbar paraspinal muscles. Journal of neuroscience methods, 2005; 145: 145-50.

Steigerwald F, Potter M, Herzog J, Pinsker M, Kopper F, Mehdorn H, Deuschl G, Volkmann J. Neuronal activity of the human subthalamic nucleus in the parkinsonian and nonparkinsonian state. J Neurophysiol, 2008; 100: 2515-24.

Tagluk ME, Sezgin N. A new approach for estimation of obstructive sleep apnea syndrome. Expert Systems with Applications, 2011; 38: 5346-51.

Trottenberg T, Kupsch A, Schneider GH, Brown P, Kuhn AA. Frequency-dependent distribution of local field potential activity within the subthalamic nucleus in Parkinson's disease. Exp Neurol, 2007; 205: 287-91.

Ubeyli ED. Time-varying biomedical signals analysis with multiclass support vector machines employing Lyapunov exponents. Digit Signal Process, 2008; 18: 646-56.

Wang S, Chen Y, Ding M, Feng J, Stein JF, Aziz TZ, Liu X. Revealing the dynamic causal interdependence between neural and muscular signals in Parkinsonian tremor Journal of the Franklin Institute, 2007; 344: 180-95.

Wang SY, Aziz TZ, Stein JF, Liu X. Time-frequency analysis of transient neuromuscular events: dynamic changes in activity of the subthalamic nucleus and forearm muscles related to the intermittent resting tremor. Journal of neuroscience methods, 2005; 145: 151-8.

Weinberger M, Mahant N, Hutchison WD, Lozano AM, Moro E, Hodaie M, Lang AE, Dostrovsky JO. Beta oscillatory activity in the subthalamic nucleus and its relation to dopaminergic response in Parkinson's disease. Journal of Neurophysiology, 2006; 96: 3248-56.

Wiley RG, Schwarzlander H, Weiner DD. Demodulation procedure for verywide-band FM. IEEE Transactions on Communications, 1977; 25: 318-27.

Wu DF, Warwick K, Ma Z, Gasson MN, Burgess JG, Pan S, Aziz TZ. Prediction of Parkinson's Disease Tremor Onset Using a Radial Basis Function Neural Network Based on Particle Swarm Optimization. Int J Neural Syst, 2010; 20: 109-16.

Zaidel A, Spivak A, Grieb B, Bergman H, Israel Z. Subthalamic span of beta oscillations predicts deep brain stimulation efficacy for patients with Parkinson's disease. Brain : a journal of neurology, 2010; 133: 2007-21.

Zaidel A, Spivak A, Shpigelman L, Bergman H, Israel Z. Delimiting Subterritories of the Human Subthalamic Nucleus by Means of Microelectrode Recordings and a Hidden Markov Model. Movement Disord, 2009; 24: 1785-93.